ELSEVIER

Biophysical Chemistry 130 (2007) 65–75

Biophysical Chemistry

http://www.elsevier.com/locate/biophyschem

Is there a difference in metal ion-based inhibition between members of thionin family: Molecular dynamics simulation study

Svetlana Oard [a,*], Bijaya Karki [b], Frederick Enright [c]

[a] LSU AgCenter Biotechnology Laboratory, Louisiana State University, 115 Wilson Bldg., LSU, Baton Rouge, LA 70803, United States
[b] Department of Computer Science, Louisiana State University, Baton Rouge, LA 70803, United States
[c] Department of Veterinary Science, Louisiana State University, Baton Rouge, LA 70803, United States

Received 22 May 2007; received in revised form 18 July 2007; accepted 19 July 2007
Available online 1 August 2007

Abstract

Thionins have a considerable potential as antimicrobial compounds although their application may be restricted by metal ion-based inhibition of membrane permeabilizing activity. We previously reported the properties associated with the proposed mechanism of metal ion-based inhibition of β-purothionin. In this study, we investigated the effects of metal ions on α-hordothionin which differs from β-purothionin by eight out of 45 residues. Three of the differing residues are thought to be involved in the mechanism of metal ion-based inhibition in β-purothionin. The structure and dynamics of α-hordothionin were explored using unconstrained molecular dynamics (MD) simulations in explicit water as a function of metal ions. Although the global fold is almost identical to that of β-purothionin, α-hordothionin displays reduced fluctuating motions. Moreover, α-hordothionin is more resistant to the presence of metal ions than β-purothionin. Mg^{+2} ions do not affect α-hordothionin, whereas K^{+} ions induce perturbations in the α2 helix, modify dynamics and electrostatic properties. Nevertheless, these changes are considerably smaller than those in β-purothionin. The proposed mechanism of metal ion-based inhibition involves the hydrogen bonding network of Arg5–Arg30–Gly27, which regulates dynamic unfolding of the α2 C-end which is similar to β-purothionin response. The key residues responsible for the increased resistance for α-hordothionin are Gly27 and Gly42 which replace Asn27 and Asp42 involved into the mechanism of metal ion-based inhibition in β-purothionin. Comparison of MD simulations of α-hordothionin with β-purothionin reveals dynamic properties which we believe are intrinsic properties of thionins with four disulphide bonds.

Keywords: Antimicrobial activity; Metal ions; Molecular dynamics simulations; β-Purothionin; α-Hordothionin; Thionins

1. Introduction

Thionins, a family of highly basic plant antimicrobial peptides, have demonstrated a broad spectrum of antibacterial and antifungal activity [1,2]. One of most studied thionins is β-purothionin (βPTH) from the wheat endosperm. The antibacterial and antifungal activity of this peptide is significantly higher than that caused by melittin or cecropin B [2,3]. Because thionins act by permeabilizing microbial membranes, there is less likelihood that target microbes will develop resistance to these peptides [1,4,5]. The thionins, therefore, hold considerable promise as class of new antimicrobial pharmaceuticals.

Thionins consist of 45–47 residues bound by three to four disulfide bonds defining high similarity of tertiary structure. Structures of several member of the thionin family including α_1-purothionin, βPTH, and β-hordothionin (βHTH) reveal a global Γ fold consisting of an arm and stem with a substantial groove in-between [6–8]. The stem is formed by two antiparallel α-helices and the arm by a coil in extended conformation, b-turns T1 and T2, and an antiparallel β-sheet consisting of two β-strands (Figs. 1A, 2A). The presence of the phosphate-and the glycerol-binding sites suggest phospholipid membrane permeabilizing activity of thionins although their mechanism of membrane disruptive activity has yet to be determined [1,6,7]. The main contributors of the phosphate-binding site include Lys1 and Arg10 with possible participation of Lys45 and Pro44. The OH groups of Ser2 and Tyr13 form the

* Corresponding author. Tel.: +1 225 578 7865; fax: +1 225 578 7863.
E-mail address: soard@agctr.lsu.edu (S. Oard).

0301-4622/$ - see front matter © 2007 Elsevier B.V. All rights reserved.
doi:10.1016/j.bpc.2007.07.005

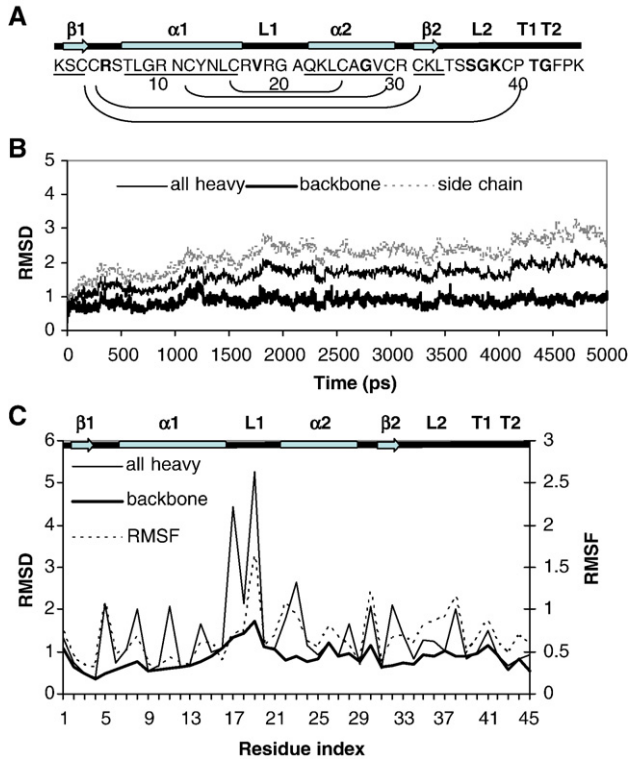

Fig. 1. MD simulation of αHTH in explicit water at 300 K. (A) Amino acid sequence of αHTH with secondary structure elements determined by X-ray crystallography for βHTH are shown above the sequence and underlined. The loops and b-turns are labeled L and T, respectively, and the disulfide bonds are shown by brackets. The amino acid residues which differ from those in βPTH are shown in bold. (B) Time evolution of RMS Deviations (in Å) between the MD trajectory and the initial crystal structure during the five-ns simulation. RMSD for all heavy (continuous line), the side chain (dashed line), and the backbone (heavy continuous line) atoms of the solute. (C) RMSD and RMS Fluctuations (in Å) as functions of residue indices. The ahRMSD (continuous line), the bbRMSD (heavy continuous line), and RMSF (dashed line) computed over the last 3 ns. Schematic representation of the secondary structure for the crystal structure is shown above the plot in correspondence with residue indices.

glycerol-binding site, while evidence of glycerol binding by Arg17 and Gln22 is inconsistent. Lys1, Arg10, Ser2, Tyr13, and Arg17 are highly conserved in the thionin family [1,9]. Ans11 and Asn14 also are conserved and stabilize formation of a homodimer through intermolecular hydrogen bonds.

Mono- and divalent metal ions inhibit membrane permeabilizing activity of thionins. Two to five mM Ca^{2+} completely blocks activity of βPTH, although 50 mM concentrations of monovalent ions like Na^{+} and K^{+} are necessary for inactivation [3,10]. Recently, a series of MD simulations were performed to determine effects of temperature and the metal ions on structure and dynamics of βPTH [11]. The MD simulations predicted that addition of K^{+} and Mg^{+2} ions in the concentrations inhibiting antimicrobial activity induces large conformational changes in the α2 helix, altering the hydrophobic region between the α-helices. Mg^{+2} ions cause larger structural and dynamic changes than K^{+} ions and greatly reduce the pK_a of Arg30. Unfolding of the α2 is triggered by altering interactions between Lys5 and Arg30 which form a hydrogen bonding network Aps42–Lys5–Arg30–Asn27 in the absence of metal ions. This hydrogen bonding network is not found in the βPTH crystal structure [7], but the MD simulations suggest that it is important for maintaining the intact α2 helix in aqueous environment. None of the network residues are highly conserved nevertheless the study on the thionin from *P. pubera* (PpTH) suggests an important role of Arg30. The D32R mutant of PpTH, whose Arg32 corresponds to Arg30 in βPTH, was shown to significantly increase antimicrobial activity as compared to the wild peptide [12]. Metal ions also reduce plasticity of the Γ fold in βPTH that modifies a steric environment of Tyr13 and could contribute to inhibiting effects of metal ions [11].

One of thionins found in wheat seed has 100% homology with α-hordothionin from barley seed (αHTH) [13] and displays high antifungal activity [14]. The peptide (αHTH from here on), differs from βPTH by eight out of 45 residues. None of the varying residues belong to the conserved primary regions; however, three of them, at positions 5, 27, and 42 are involved in the mechanism of metal ion inhibition in βPTH [11]. This fact predicts considerable differences in the response of αHTH to the presence of metal ions in comparison with βPTH.

In this work, we investigated the key properties of αHTH using unconstrained MD simulations in explicit water as a function of the presence of metal ions. Results of MD simulations

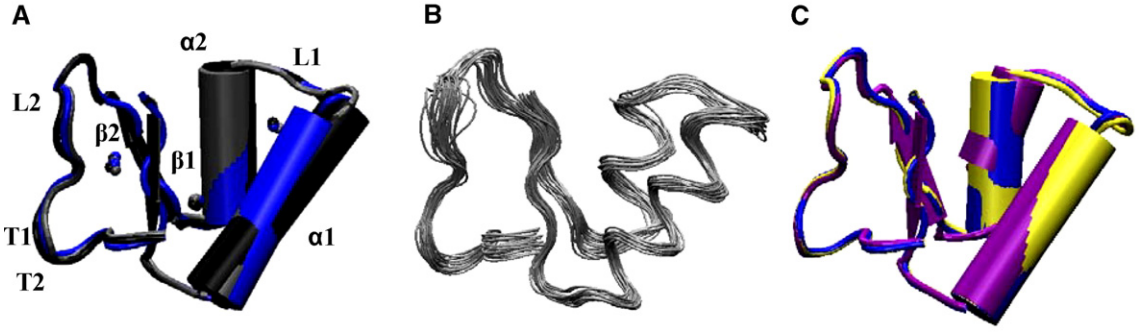

Fig. 2. Structure of αHTH. (A) Superposition of the average αHTH MD structure (blue) with the βHTH crystal structure (gray) and the average βPTH MD structure (black) with the disulfide bonds shown as connected spheres. (B) Snapshots of the αHTH MD structures taken with 100-ps intervals between 3 ns and 5 ns. (C) Superposition of the average αHTH MD structures without metal ions (blue) and in the presence of K^{+} (purple) or Mg^{+2} ions (yellow).

suggest that αHTH is more resistant to the presence of metal ions than βPTH. Comparison of MD trajectories of αHTH and βPTH at different conditions provides new insights in the mechanism of metal ion-based inhibition and future directions for developing metal ion-resistant thionins.

2. Computational methods

2.1. Molecular model and computational methodology

Because the crystal structure of α-hordothionin from barley seed (αHTH) [13] has not been determined, the initial αHTH structure was obtained from the X-ray structure of barley β-hordothionin (βHTH) with a PDB entry code 1WUW which was determined at 1.9 Å and pH 5.6 [8]. All water and ligand molecules determined by crystallography were removed. The residues different from those in αHTH were changed using AMBER-8 software package. Six residues were mutated to produce the αHTH primary sequence: N27G, A27V, G36S, L37S, S41T, and S42G. MD simulations were performed using the Peach 5.8 software package [15] and the flexible, single point charge (fSPC) water potential [16]. To adequately represent our experimental model and produce reliable results, simulation parameters were optimized as previously described [11], insuring accurate computations of electrostatic and interaction energies with metal ions.

The simulation box was neutralized by adding 10 Cl^- ions. Minimization of the system was performed in four steps. First, only mutated solute atoms were minimized. Then water molecules were completely minimized followed by minimization of water together with ions. Finally, all atoms were minimized for 100 steps. Equilibration started with heating and equilibrating water and ions only as described before [11] at 325 K for 500 ps. The entire system was equilibrated at 325 K for 1 ns. To study evolution of the molecular structure and stability, αHTH was simulated for 5 ns at 300 K in explicit water.

Interactions of the peptide with metal ions were simulated at 300 K in the presence of 100 mM K^+ ions or 20 mM Mg^{+2} ions [3,12]. Concentrations of metal ions were chosen based on the experimental data to fully inhibit antimicrobial activity of βPTH [3,10]. Because the initial structure of αHTH was obtained through mutating the crystal structure of βHTH, the average αHTH MD structure was selected as the initial structure for MD simulations in the presence of metal ions. The average αHTH structure was obtained from the MD trajectory in the absence of metal ions by averaging over 500 ps after the equilibration of the αHTH structure was completed. Validitation of the 500-ps average structure as the starting structure was confirmed by superposing the former with the average structures and two snapshots for each of five consecutive 100 ps-periods. The simulation boxes were prepared as described above. To reach corresponding concentrations, the 9 K^+ or 2 Mg^{+2} ions were added to the simulation box with αHTH, and the chloride ions were added proportionally to neutralize the system. After minimization and equilibration as above, the systems were simulated at 300 K for 2 ns.

2.2. Analysis

Analysis of the MD trajectories was performed using Peach 5.8 [15] and Amber-8 [17]. Convergence of MD trajectories was assessed by averaging the all heavy solute atom RMSD values for all heavy solute atoms from the initial structure over 100-ps intervals. To calculate average structures, root mean square difference (RMSD) for all heavy atoms, backbone N, CA, and C atoms, and side chain atoms and root mean square fluctuation (RMSF), average solvent-accessible area (SAA), and hydrogen bonds, the last two or 3 ns of MD trajectories with or without metal ions, respectively, were used. Secondary structures were defined with the DSSP program [18]. The pK_a shifts were calculated as described [11] with the electrostatic potential obtained using the Adaptive Poisson–Boltzmann Solver software package (http://mccammon.ucsd.edu/apbs). For visualization of structures and trajectories, the VMD1.8.3 was used [19].

3. Results

3.1. Structure and dynamics of αHTH

The MD trajectory of αHTH at 300 K in the absence of metal ions (αHTH-300K) was structurally stable for the entire 5-ns period (Fig. 1). The peptide reached equilibrium after 1500 ps of the MD simulation according to the convergence test. The extended equilibration time may be related to mutating six residues in the initial structure to obtain the primary sequence of αHTH from the βHTH crystal structure. After reaching equilibrium, the RMSD from the crystal structure fluctuated around 0.9 Å for the backbone (bbRMSD) and 1.8 Å for all heavy atoms (ahRMSD) (Fig. 1B). No significant structural changes were found during the entire simulation (Fig. 2B).

The αHTH MD structure has general features of the Γ fold characteristic for thionins [4,7]. The superposition of the average αHTH MD structure with the crystal βHTH and βPTH MD structures displays a good fit for the secondary structures (Fig. 2A). Differences are observed in the loop regions, β-sheet and the C-end of the α1 helix. The β-sheet in the αHTH MD structure is weakly defined unlike in the βHTH and βPTH structures. The α1 C-end in the average αHTH MD structure as in βHTH is shorter than that in βPTH. The DSSP analysis confirms substantial similarity between secondary structures of the αHTH MD and the crystal βHTH structures (Table 1).

The bbRMSD values indicate small conformational differences between the αHTH and the initial structural backbones, including the loop regions (Fig. 1C). The ahRMSD values show that conformational variance is restricted primarily to the side chains of charged residues. Interestingly, Arg17 and Arg19 in the L1 loop substantially deviate from the initial structure with ahRMSD around 5. The same residues had the largest ahRMSD values in the βPTH MD structure [11]. The RMSF values indicate that the α1 helix is the most rigid region in the peptide while the α2 helix is dynamic, especially the α2 N-end. Similar discrepancy in mobility between the α1 and the α2 helice were found in βPTH [11]. Interestingly, Arg5 and Arg30 belong to

Table 1
Comparison of the secondary structure of αHTH with βPTH and βHTH at different conditions

Peptide		Conditions	α-Helix	β-Sheet	Other
β-HTH	CrS [a]	289 K	0.38 (7–16, 22–28) [b]	0.13	0.49
α-HTH	MD	300 K	0.38 (7–16, 22–28)	0.09	0.53
	MD	300 K, K^+	0.33 (7–16, 22–26)	0.13	0.54
	MD	300 K, Mg^{+2}	0.38 (7–16, 22–28)	0.09	0.53
β-PTH	CrS [c]	RT, Mg^{+2}	0.38 (7–16, 22–28)	0.13	0.49
	MD [d]	300 K	0.40 (7–15, 22–29)	0.13	0.42
	MD	300 K, K^+	0.38 (7–19, 26–29)	0.13	0.42
	MD	300 K, Mg^{+2}	0.40 (7–17)	0.13	0.56

[a] Crystal structure [8].
[b] Residue indices forming a secondary structure are given in brackets.
[c] Crystal structure [7].
[d] βPTH MD structures [11].

the most dynamic residues in αHTH with RMSF values above 1. However, the corresponding residues in the βPTH MD structure, Lys5 and Arg30, display only moderate mobility with RMSF values around 0.5 [11]. The L2 loop and b-turns display elevated fluctuations which are, however, considerably smaller than those in the βPTH MD structure [11]. In the L1 loop, the Arg19 side chain generates large fluctuating motions reaching RMSF value of 1.8.

The strong hydrogen bonds between Cys4, Lys45, Arg10, and Ser2 connect the arm and stem into the Γ fold (Table 2). This hydrogen bonding network at the inner corner of the Γ is very similar to that of the βPTH crystals [7] and the βPTH MD structure [11]. In contrast, a hydrogen bonding network at the outer corner of the Γ, Arg5–Arg30–Gly27, is considerably weaker and shorter as compared to the strong Lys5–Gln27–Arg30–Asp42 network found in βPTH [11]. A weak hydrogen bond is found between Arg30-NH1 and Gly27-O. Arg5 interacts with Arg30 instead of Gly42 through a weak hydrogen bond Arg5-NE:Arg30-O. The weak hydrogen-bonding network may explain the increased RMSF values for Arg5 and Arg30 observed in the αHTH-300 K trajectory.

In the αHTH-300 K trajectory, αHTH undergoes considerable vibrational motions. The three-residue antiparallel β-sheet (1–3, 32–34) is highly dynamic. When completely expanded and therefore tightly bound, it has four hydrogen bonds. The N-end of the β-sheet in the αHTH-300K trajectory continuously undergoes rapid reversible unzipping to the two residue state. The tightly bound state lasts only for 1–2 ps alternating with the two residue state which lasts from 3 to 20 ps. Changes in the distance between Thr34-O and Lys1-N demonstrate dynamics of unzipping of the β-sheet N-end while the distance between Cys3-O and Lys32-N illustrates the relative stability at the C-end of the β-sheet (Fig. 3A,B).

The α2-helix is another flexible region in the peptide. The α2 C-end is particularly dynamic with periodical and reversible unfolding for 1–2 ps on average once every 30–80 ps. In addition, the α2 helix goes through several complete disruptions and reformations during the course of the MD simulation, although these motions are rare as compared to partial unfolding. These perturbations last from 5 to 15 ps each. Changes in distance between Leu24-O and Val28-N illustrate unfolding/folding motions in the α2 C-end region with ~3 Å corresponding to the folded state, and the distance increases between Gln22-O and Ala26-N that correspond to unfolding of the entire helix (Fig. 3C,D).

3.2. Effect of mono- and divalent metal ions

Presence of both K^+ and Mg^{+2} ions triggers conformational and dynamic changes in αHTH. Mg^{+2} ions induce mild changes while K^+ ions significantly perturb the peptide conformation in the α2 helical region. The final ahRMSD from the initial structure for the MD trajectories with K^+ (αHTH-K) and Mg^{+2} (αHTH-Mg) ions are 1.8 Å and 1.6 Å, respectively. The average bbRMSD values do not differ significantly among all three trajectories although the bbRMSD values fluctuate more in the αHTH-Mg and especially the αHTH-K MD trajectory than in the αHTH-300K trajectory reflecting conformational perturbations (Fig. 4A).

The superposition of the average MD structures without and in the presence of metal ions displays differences in effects of K^+ and Mg^{+2} ions on αHTH (Fig. 2C). The αHTH-Mg structure is nearly identical to the αHTH-300K structure. In contrast, the αHTH-K structure has the unfolded C-end of the α2 helix and longer β-sheet than the αHTH-300 K, although the α1 helix, b-turn, and loop regions remain unperturbed. Summary of effects of K^+ and Mg^{+2} ions on secondary structures is presented in Table 1. Thus, secondary structures of αHTH show higher resistance to the presence of metal ions than that of βPTH whose secondary structures are largely affected by both K^+ and Mg^{+2} ions [11].

RMSD and RMSF values for each residue in the MD trajectories without and with metal ions are compared in Fig. 4. Mg^{+2} ions induce smaller conformational changes in the backbone and side chains of αHTH than K^+, considerably elevating only the Arg19 bbRMSD. K^+ ions induce an increase of the bbRMSD values in the entire α2 helix and of Arg30. Both metal ions significantly increase the ahRMSD values for Arg30 and Lys38, and K^+ ions, in addition, increase the ahRMSD for Lys5 and Lys23. Both cations have very little effect on the α1 helix and b-turn residues. Effects of metal ions on RMSF values

Table 2
Fraction of hydrogen bonds in MD simulations of αHTH at different conditions

Hydrogen bonds		% [a]		
Donor	Acceptor	300 K	300 K, K^+	300 K, Mg^{+2}
Cys4-N	Lys45-O	84	83	87
Lys45-N	Cys4-O	44	38	47
Arg10-NE	Lys45-OT	84	90	95
Arg10-NH2	Lys45-O	93	90	88
Arg10-NH2	Lys45-OT	12	15	16
Arg10-NH1	Ser2-OG	69	57	59
Arg10-NH2	Ser2-O	61	73	74
Arg5-NE	Arg30-O	35	0	32
Arg5-NH1	Gly42-O	0	45	10
Arg30-NH1	Gly27-O	18	9	24
Arg17-NH2	Asn14-OD1	41	57	9

[a] A hydrogen bond is considered if the donor–acceptor distance is smaller that 3 Å and the donor–hydrogen–acceptor angle is larger than 135°.

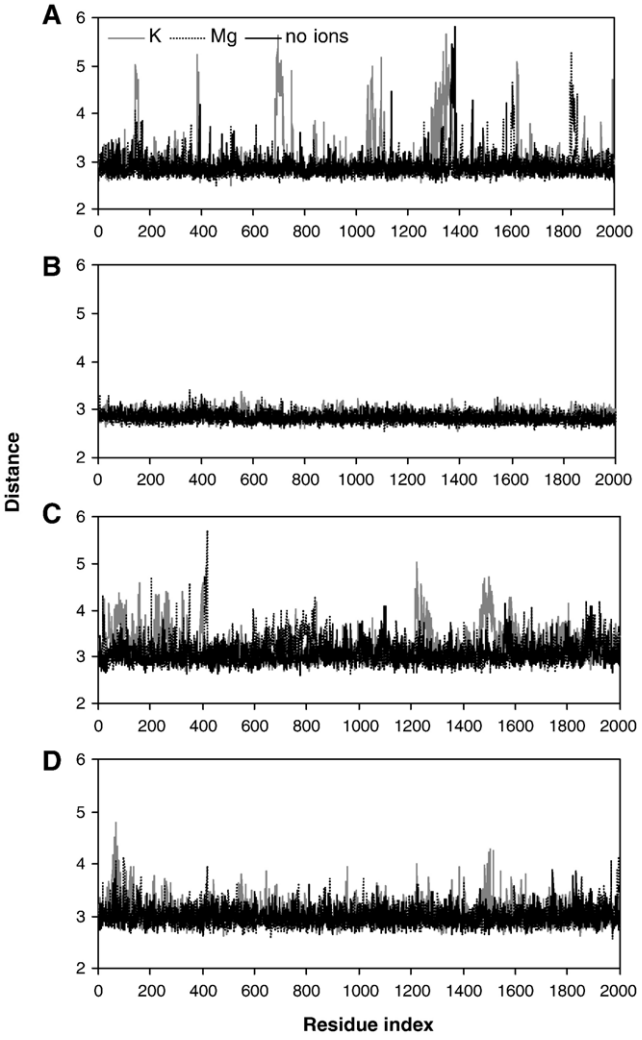

Fig. 3. Metal-ion-dependent changes in distance between the β1 and β2 strands in the antiparallel β sheet and within the α2 helix. Time evolution of distances (in Å) between (A) Thr34-O and Lys1-N, (B) Cys3-O and Lys32-N, (C) Leu24-O and Val28-N, and (D) Gln22-O and Ala26-N atoms for the MD trajectories with no metal ions present (black line), with 100 mM K^+ (gray line), and with 20 mM Mg^{+2} ions (dashed line). Last 2 ns of the MD trajectory with no metal ions present are shown.

are consistent with conformational changes. Mg^{+2} ions cause smaller changes in the peptide dynamics than K^+ ions. Mg^{+2} ions induce a large increase in fluctuating motions of only Arg17 while K^+ ions increase RMSF values for the entire α2 helix and the L2 loop. Interestingly, both metal ions elevate fluctuating motions of Arg30. Comparison of effects of metal ions on αHTH RMSD and RMSF values with those obtained for βPTH [11] unambiguously point to higher resistance of αHTH to metal ions.

Both metal ions have no significant effects on the hydrogen bonds that form the Γ (Table 2). In the αHTH-Mg trajectory, the hydrogen bonds on the outer corner of the Γ are maintained similarly to that in the αHTH-300 K trajectory. However, in αHTH-K, Arg5 forms a weak hydrogen bond with Gly42-O instead of the hydrogen bond with Arg30-O observed in the αHTH-300 K structure. The total SAA of backbone atoms and of side chain atoms are not affected by the presence of both metal ions (data not shown). However, several residues significantly change SAA values upon addition of metal ions (See Supplementary material, Fig. 1). In particular, both the backbone and the side chain SAA of the conserved residue-Tyr13 are significantly higher in the αHTH-Mg than in the αHTH-300 K trajectory while no changes are found in the αHTH-K trajectory.

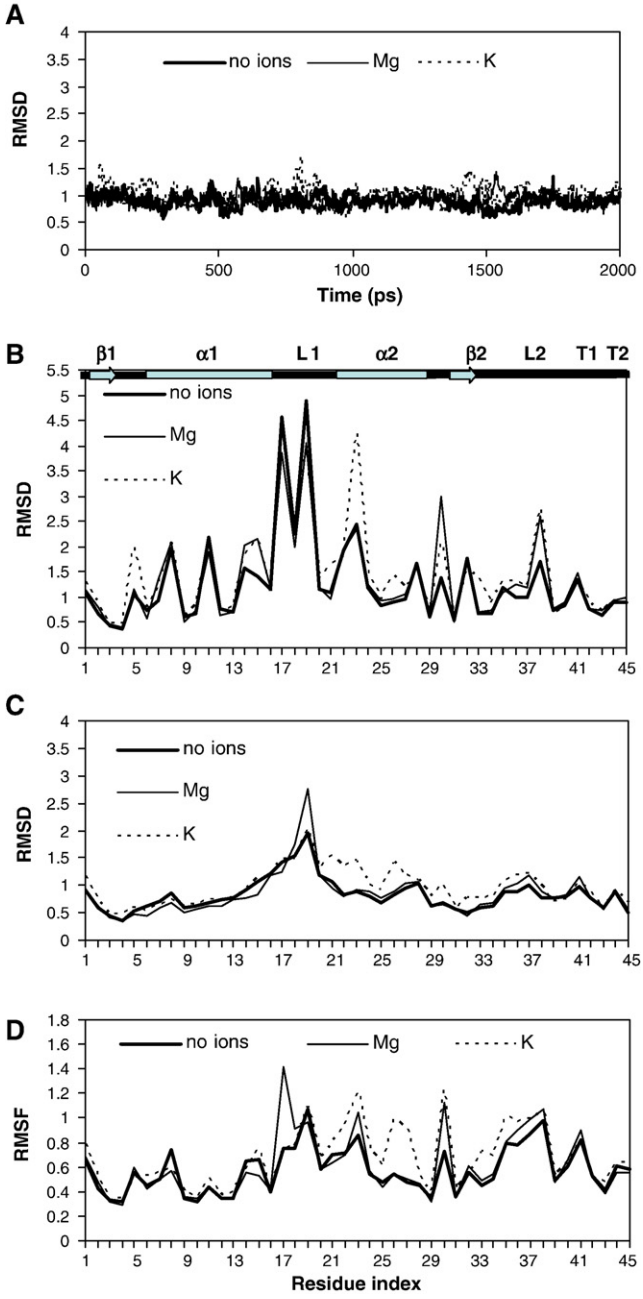

Fig. 4. Effects of K^+ and Mg^{+2} ions on structure and dynamics of αHTH (in Å). (A) Time evolution of bbRMSD between the MD trajectories without metal ions (heavy continuous line), with 100 mM of K^+ (dashed line), and with 20 mM Mg^{+2} (continuous line) and the initial crystal structure during the last 2 ns of MD simulations. (B–D) RMSD and RMSF as functions of residue indices. (B) ahRMSD and (C) bbRMSD between the MD and the initial crystal structures, and (D) RMSF for the MD trajectories without metal ions, with K^+, and with Mg^{+2} ions . The average values were calculated over the last 2 ns of simulations. Schematic representation of the secondary structure as in Fig. 1C.

Mg^{+2} has only a small effect on the peptide dynamics while K^+ ions greatly modify vibrational motions in the β-sheet and α2 helix. In the αHTH-Mg trajectory, the main difference consists of the 140-ps-long perturbation in the α2 where the helix undergoes several unfolding/folding cycles which occur between 600 and 740 ps of the MD simulation. In the αHTH-K trajectory, the β-sheet becomes more stable and the dynamics observed in the αHTH-300 K trajectory is dominated by extended periods of the tightly bound state and the two residue state lasting from 20 to 80 ps each. Comparison of the distances betweenThr34-O and Lys1-N as well as between Cys3-O and Lys32-N illustrates changes in the β-sheet dynamics in the presence of metal ions (Fig. 3A,B). The α2 C-end becomes predominantly unfolded in the presence of K^+ions. Moreover, the entire α2 helix frequently unfolds for 1 to 4 ps. Frequencies of the structural alterations in the α2 C-end and the entire α2 helix are reflected in the increases of distances between Leu24-O and Val28-N and between Gln22-O and Ala26-N, respectively (Fig. 3C,D).

3.3. Dihedral angles

To understand conformational perturbations in the α2 helix, the time evolution of the dihedral angles and side-chain conformations in the absence and presence of metal ions was analyzed. The major differences between the αHTH-300K,

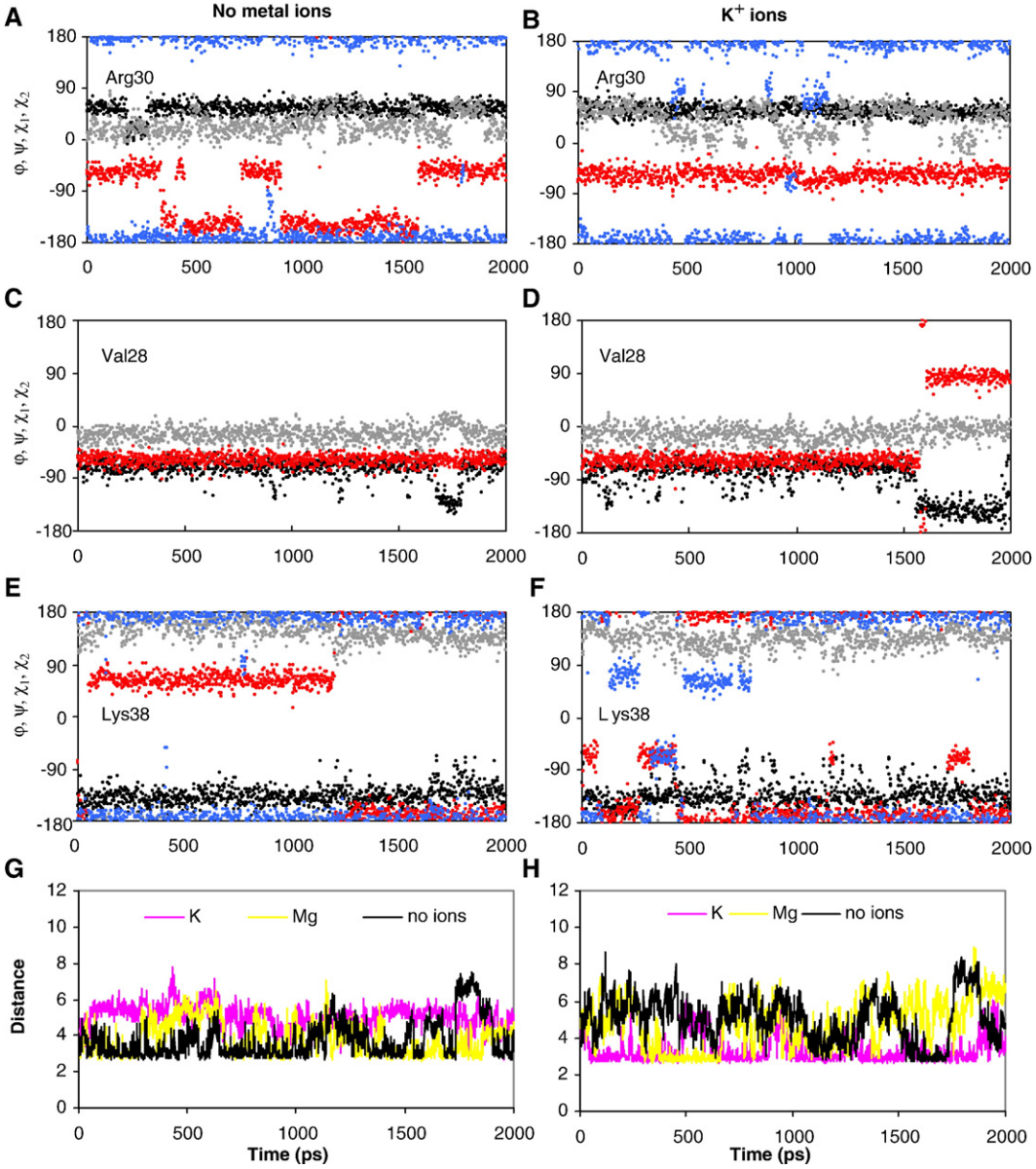

Fig. 5. Time evolution of conformational changes induced by the presence of K^+ ions during the last two ns. (A–F) φ (black dots) with ψ (gray dots) represent backbone dihedral angles, and χ_1 (red dots) with χ_2 (blue dots) represent side-chain dihedral angle values of residues (A, B) Arg30, (C, D) Val28, and (E, F) Lys38 in the MD trajectories (left graphs) without metal ions and (right graphs) with 100 mM K^+ions. Distance (in Å) (G) between Arg5-NE and Arg30-O and (H) between Arg5-NH1 and Gly42-O atoms in the MD trajectories without metal ions (heavy continuous line), K^+ (dashed line), and Mg^{+2} (continuous line).

αHTH-K, and αHTH-Mg trajectories are found for the φ and ψ backbone dihedral angles of Gly27, Val28, Arg30, Ser36, and Lys38. The φ and ψ of Arg30, Ser36, and Lys38 exist in αHTH-300K in the predominant and the transient conformations that indicate increased flexibility of their backbones. Arg30 has a flexible backbone with the predominant and transient (φ,ψ) values of (55°,30°) and (55°,50°), respectively (Fig. 5). Lys38 and Ser36 exist primarily in the (−140°, 130°) and (−60°,150°) conformations, respectively. Both metal ions, especially K^+ ions increase frequency of the transient conformations for all three residues. However, the predominant and transient (φ,ψ) values remain unaffected. The exception is Arg30 whose transitional conformation becomes predominant in the presence of K^+ ions. Notably, perturbations of the Arg30 ψ angle are consistent with changes in the interactions between Arg30 and Arg5. In the αHTH-300 K trajectory, Arg30 forms a weak hydrogen bond with Arg5, and increases in the distance between Arg30-O and Arg5-NE correspond to shifts in the Arg30 ψ angle (Fig. 5G,H). In the αHTH-K trajectory, Arg30 interacts mainly with Gly42, and no correspondence with perturbations in the Arg30 dihedral angles is observed despite large perturbations of the Arg30 ψ angle.

In the αHTH-300K trajectory, Gly27 and Val28 assume two distinct conformations corresponding to the folded and unfolded α2 C-end. Gly27 takes the values of (−75°,−55°) and (−130°,10°), and Val28 values of (−70°,−15°) and (−135°,5°), for the folded and unfolded states, respectively. Mg^{+2} ions do not considerably modify φ and ψ dihedral angles of Gly27 and Val28 while K^+ ions increase frequency of angles corresponding to the unfolded state. Interestingly, the Cys29 ψ dihedral angle undergoes small arch-like shifts associated with unfolding of the α2 C-end in all trajectories. In the αHTH-K trajectory, the Cys29 backbone is affected even more because its ψ dihedral angle undergoes several shifts as well.

The side-chain conformations of Val28, Arg30, and Lys38 are most affected by the presence of metal ions (Fig. 5). The Arg30 χ_1 rotamer found in the αHTH-300 K trajectory explores two conformations with the (φ,ψ,χ_1) values at (55°,30°,−60°) and (55°,30°,−170°) which have high probabilities according to the backbone–dependent (BBD) rotamer library [20]. In the

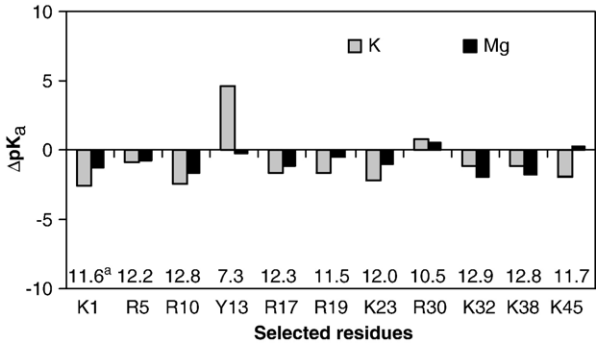

Fig. 6. pK_a shifts in the presence of K^+ and Mg^{2+} ions for the selected ionizable residues. The Δ pK_a were calculated as differences between the pK_a calculated for the residues in the averaged MD structures with cations and with no cations added. Δ pK_a for K^+ ions (gray) and for Mg^{2+} ions (black). [a]The intrinsic pK_a values in the averaged MD structure in the absence of metal ions are given above each residue.

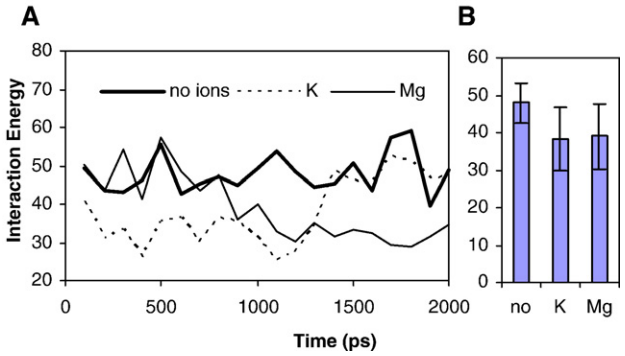

Fig. 7. Interaction energy (in Kcal/mol) between the residues Arg5 and Arg30. (A) Time evolution of interaction energy in the MD trajectories with no metal ions (heavy continuous line), K^+ ions (dashed line), and Mg^{2+} ions (continuous line). (B) Average values of interaction energy with standard deviations in the MD trajectories with no metal ions (no), K^+ ions (K), and Mg^{2+} ions (Mg) computed over the last 2 ns.

αHTH-K trajectory, the Arg30 χ_1 rotamers change to (55°,60°, −60°) and (55°,10°,−60°). The later conformation has 0 probability according to the BBD library. Its (χ_1, χ_2) pair has the (−60°, 60°) value which is rare as well in the backbone-independent library. Similarly, the Val28 χ_1 rotamer in the αHTH-300 K trajectory has highly probable conformations, but changes to the rare conformation (−135°,−5°,90°) in the αHTH-K after 1500 ps. Mg^{+2} ions have no effect on the Arg30 and Val28 χ_1 rotamers. Both the χ_1 and χ_2 Lys38 rotamers undergo frequent changes in the αHTH-Mg and especially the αHTH-K trajectory. The χ_1 rotamers and the (χ_1, χ_2) pairs for all other residues in both the trajectories without and with metal ions explore highly probable conformations and have similarity to each other.

Thus, Arg30 is maintained in the usual conformation in αHTH, and the Arg30 side chain assumes the rare conformation only in the presence of K^+ ions unlike in βPTH. Effects of both mono-and divalent ions on dihedral angles and side-chain conformations in αHTH are considerably smaller than those observed in βPTH [11].

3.4. Electrostatic effects

Our calculations performed on the αHTH-300K structure indicate that αHTH bears large positive charge because the peptide not only has ten basic residues, but also seven out of ten basic residues have elevated pK_a values, especially Lys32 and Lys38 (Fig. 6). These lysines and arginines have high probability of being protonated at neutral pH contributing to a large total positive charge on αHTH. Two residues, Arg30 and Tyr13, have lower than expected pK_a values of about 10.5 and 7.3, respectively. Both residues are located in the center of the Γ fold, Arg30 at the outer corner and Tyr13 at the inner corner. In the case of Try13, such a low pK_a may occur due to embedding of Tyr13 in the peptide core.

The intrinsic pK_a shifts induced by metal ions are presented in Fig. 6. The intrinsic pK_a values were calculated with all explicit ions removed from the MD trajectories, and therefore reflect conformational changes induced by metal ions. The pK_a

calculations indicate that both metal ions reduce the total positive charge on the peptide, especially K^+. Mg^{+2} ions reduce pK_a values by more than two only for Lys32 and Lys38, whereas K^+ ions significantly reduce pK_a of Lys1, Arg10, Lys23, and Lys45 and markedly increase the pK_a of Tyr13. In general, these changes are not sufficient to change ionization states of the above residues. However, pK_a of Tyr13 increases by about 4.6 in the presence of K^+ions. Such a large positive pK_a shift indicates that Tyr13 becomes mainly protonated at neutral pH. This increase can not be explained by changes in exposure to the solvent because the SAA values for Tyr13 are identical in the ÇαHTH-300 K and αHTH-K trajectories (see Supplementary material, Fig. 1). Interestingly, Arg30 undergoes only small positive pK_a shifts in the presence of both metal ions. In βPTH, Mg^{+2} ions induce a large decrease in pK_a of Arg30 and affect other ionizable residues more than K^+ions [11]. But in αHTH, Mg^{+2} ions have a small effect on pK_a of ionizable residues while K^+ ions shift pK_a values, although shifts are considerably smaller than in βPTH.

3.5. Ion distribution

To study interactions of metal ions with αHTH, we analyzed anion and cation distributions in all trajectories. Cl^- ions move freely in all MD trajectories and do not become associated with any particular residue, although periodically coming within 3 Å from the peptide. K^+ ions are primarily associated with Cl^- ions in the αHTH-K trajectory and rarely come within 5 Å of the peptide. In contrast, divalent cations do not approach αHTH. Each Mg^{+2} ion becomes tightly associated with a Cl^- ion and pentahydrated in the αHTH-Mg trajectory. These results are consistent with the experimental data because no a particular binding site was found for Mg^{+2} ions in the βPTH crystal structure despite a high concentration of Mg^{+2} ions during crystallization [7]. Moreover, similar behavior of Mg^{+2} ions was found in the MD trajectory of βPTH [11].

According to the ion density maps (see Supplementary material, Fig. 2), Cl^- ions are found in the peptide vicinity in the αHTH-300K trajectory mainly in three areas: at the N-termini of the α2 helix with a large ion density at Lys23, at the L2 loop with the largest density at Lys38, and along the groove of the Γ fold at the C-terminus. The presence of K^+ ions results in the large increase of the Cl^- density at Arg30 in addition to the areas found in the absence of metal ions. Mg^{+2} ions change Cl^- distribution around αHTH by stretching ion densities at the α2 N-termini between Gln22 and Leu24 and increasing ion densities at the loop L1, in particular, at Arg17 and Arg19. Mono- and divalent ions show no similarity in ion density distribution around αHTH. K^+ ions closely follow Cl^-ions with the largest K^+ ion densities at Lys23, Lys38, and Lys45. The largest Mg^{+2} ion density is found at Thr7 which side chain is proximal to the C-terminus and on the opposite side of the peptide at Lys32 although the density values are small in comparison with those for Cl^- and K^+ ions. Thus, the main difference lies in strong interaction of Cl^- ions with Arg30 in the αHTH–K trajectory unlike in the αHTH-300K or the αHTH-Mg trajectory.

3.6. Interaction energies

Our results indicated an increase in resistance of αHTH to the presence of metal ions as compared to βPTH. Because inhibition of βPTH by metal ions was associated with the Arg30 hydrogen bonding network, in particular with interaction between Arg30 and Lys5 which are linked together by the disulfide bonds at the α2 C-end [11], we investigated interaction energies within theArg30 hydrogen bonding network in αHTH. The interaction energies between Arg30 and Arg5 presented in Fig. 7 are consistent with the proposed mechanism of metal ion-based inhibition [11]. In the αHTH-300 K trajectory, the interaction energy between Arg30 and Arg5 is high indicating strong repulsive interactions (Fig. 7A). The interaction energy fluctuates around the average value during the course of the simulation. The presence of metal ions causes larger shifts in the interaction energy; however, there is no significant difference between interaction energies in the trajectories without metal ions present and in the presence of neither metal ions (Fig. 7B). Thus, the Arg30 network is less sensitive to the presence of metal ions than the corresponding network in βPTH. As a consequence, αHTH is more resistant to the presence of metal ions than VPTH. This result confirms an important role of the Arg30 network in the mechanism of metal ion-based inhibition of purothionins.

4. Discussion

Our explicit MD simulations predict reduced fluctuating motions and increased resistance of αHTH to the presence of metal ions as compared to βPTH [11]. Mg^{+2} ions induce only mild changes while K^+ ions significantly perturb αHTH, although the effects are smaller than in the case of βPTH. Effects of K^+ ions on αHTH are similar to effects of K^+ and Mg^{+2} ions on βPTH, namely, large conformational changes in the α2 helix, the predominantly unfolded α2 C-end, modified fluctuating motions, and a substantial reduction in total positive charge. This study confirms our hypothesis about the pivotal role of the hydrogen bonding network at the outer corner of the global Γ fold in unfolding of the α2 C-end that was postulated for βPTH. Thus, the collective simulation data for αHTH and βPTH show that the mechanism of metal ion-based inhibition of thionins involves more than electrostatic screening suggested previously [1,10]. The increased resistance of αHTH to the presence of metal ions is due to differences in the primary structure varying from βPTH by eight amino acid residues (Fig. 1A). All varying residues belong to the variable regions in the thionin family [1]. A closer look at the data obtained from the MD simulations provides insights into properties and the mechanism of metal ions-based inhibition of thionins.

Our MD simulations show that instability of the C-end of the α2 helix is an intrinsic property of αHTH as well as βPTH [11]. In the absence of metal ions, the α2 C-end is highly dynamic in both peptides and periodically unfolds with the folded state being predominant. The folded state is stabilized by the weak hydrogen bonds Arg5-NE:Arg30-O and Arg30-NH1: Gly27-O. Thus, αHTH also has a regulating hydrogen bonding network at

the outer corner of the Γ, Arg5–Arg30–Gly27. However, the αHTH regulating network is weaker and shorter than the corresponding network in βPTH, Asp42–Lys5–Arg30–Asn27 [11]. In both peptides the Arg30 regulating network involves strong repulsive interactions between two basic residues that play a central role in the network. In the case of αHTH, Arg30 is tightly bound to Arg5 by two disulfide bonds. Our computations show that this structure introduces instability through strong repulsive interactions of two arginines and constraints imposed on the Arg30 backbone atoms by the flanking Cys29 and Cys31 residues. Perturbations in the Arg5–Arg30–Gly27 hydrogen bonding network result in unfolding of the α2 C-end in αHTH as in βPTH. When the network is perturbed, the repulsive interactions between Arg30 and Arg5 side chains create structural perturbations in the Arg30 backbone atoms. Strong conformational perturbations in the Arg30 backbone radiate into the α2 C-end triggering unfolding.

Thus, the principle of the α2 C-end unfolding is the same as in βPTH despite the shorter hydrogen bonding network regulating this process and replacement of three out of four residues of the network. The crystallographic data show no evidence of the hydrogen bonding network in βPTH, βHTH, or α1-purothionin [6–8]. Nonetheless, the majority of thionins with four disulphide bonds have amino acid residues in the corresponding positions, which should form similar regulating networks. The majority have a long regulating network similar to that in βPTH, for example, in the oat avenothionin α (Asp42–Lys5–Arg30–Thr27) [21], *Tulipa gesneriana* thionin Class1 (Asp43–Arg5–Asp31–Ala28) [22], and *P. pubera* thionin (Asp44–Arg5–Lys29–Asp32) [23]. A few thionins including wheat α1-purothionin have a shortened regulating network (Arg5–Arg30–Gly27) [24] as in αHTH. Furthermore, absence of the hydrogen bonding network in the crystal strictures of βPTH, βHTH, or α1-purothionin may be explained by ligand interference. In all three crystal structures, a negatively charged ligand is found only 4–5 Å from Arg30 [6–8]. A ligand is positioned between the Arg(Lys)5 and Arg30 side chains that occur in the middle of the Arg30 network, observed in our MD trajectories.

Changes in the primary sequence from βPTH to αHTH make the peptide resistant to the presence of Mg^{+2} ions and partially increase resistance to K^{+}ions. First, replacements at positions 27, 38, 41, and 42 lead to a decrease of fluctuations in the α2 C-end, L2 loop, and b-turn resulting in overall reduced fluctuation motions in αHTH as compared to βPTH that contributes to the increased resistance to metal ions. Second, replacements at positions 5, 27, and 42, which belong to the Asp42–Lys5–Arg30–Asn27 hydrogen bonding network involved in the mechanism of metal ion-based inhibition in βPTH [11], result in the shorter and weaker regulating hydrogen bonding network, Arg5–Arg30–Gly27, that contributes to the increased resistance as well. In particular, replacement of asparagine at position 27 to glycine largely contributes to stabilization of the α2 C-end by weakening a hydrogen bond between the Arg30 side chain and Gly27-O located in the α2 C-end. Reduction in interactions between Arg30 and the α2 backbone atoms makes the α2 C-end less sensitive to the presence of metal ions as compared to βPTH which Arg30 side chain forms a strong hydrogen bond with Asn27-O. Replacement of negatively charged aspartic acid with glycine at position 42 results in the interaction of the Arg5 side chain with Arg30-O instead of Gly42. Consequently, the network regulating dynamics of the α2 C-end, Arg5–Arg30–Gly27, is shorter and weaker in αHTH than in βPTH. The weakened network weakly affects the α2 C-end; therefore the α2 helix fluctuates less in αHTH than in βPTH. Furthermore, this makes the α2 C-end less sensitive to the presence of metal ions. Our computational results are in excellent agreement with the crystallographic data which showed that the α2 helix in α1 purothionin, which hydrogen bonding network is identical to that in αHTH, is considerably less mobile than that of βPTH [7]. Replacement of hydrophobic leucine in the exposed to water L2 loop with lysine contributes to reduction of fluctuating motions at the C-terminus further stabilizing αHTH.

Thus, our results indicate that Arg30 plays an important role in regulating peptide dynamics, in particular the α2 helix in both αHTH and βPTH through the regulating hydrogen bonding network. In addition, Arg30 is among the most affected residues by both K^{+} and Mg^{+2} ions in αHTH. Addition of K^{+} ions induces a switch to rare backbone dihedral angles and side chain rotamers in Arg30 [20]. The majority of thionins with four disulphide bonds contain arginine at this position. PpTH is one of few exceptions which has aspartic acid instead [23]. Vila-Perello and coworkers showed that the D32R mutation, which corresponds to Arg30 in αHTH and βPTH, in PpTH and its shortened variant PpTH-(3–41) increases antimicrobial activity [12,25].

The crystallographic data show no evidence of Arg30 interactions with other residues; nevertheless, its side chain is among the most dynamic [6–8]. The latter is consistent with our results. Besides, our computations for the Arg30 side chain rotamers are in excellent agreement with the experimental data. In the MD trajectories in the absence of metal ions, the αHTH Arg30 side chain assumes populated rotamers while the βPTH Arg30 is maintained in the rare conformations including the structures in the presence of metal ions [11]. Similarly, the Arg30 side chain conformations were found outside allowed regions of Ponder & Richards libraries [7,26] in βPTH [7,8], but not in α1 purothionin crystal structure [6]. The latter should form the identical hydrogen bonding network, Arg5–Arg30–Gly27, with αHTH that explains the populated conformations of Arg30 in the α1 purothionin crystal structure. Moreover, the fact, that the α1 purothionin Arg30 is maintained in the populated conformations supports the presence of the network regulating the Arg30 conformation that was demonstrated in our MD simulations.

Addition of K^{+} ions triggers the large increase of pK_a of Tyr13 from 7.3 to 11.9, the largest pK_a shift in αHTH. This increase cannot be explained by changes in the solvent exposure which remains the same in αHTH-300 K and αHTH-K structures. Tyr13 is buried in the peptide core in all MD trajectories produced for αHTH and βPTH that is consistent with the crystallographic data [6–8], and its conformation is not significantly affected by metal ions. Changes in interactions with neighboring residues, in

particular, with the carboxamide group of Gln22, may be a reason for the discrepancy in pK_a values. In the αHTH-300 K trajectory, the side-chain carbonyl oxygen of Gln22 often accepts the Tyr13 hydroxyl hydrogen via the hydrogen bond. Meanwhile, in the αHTH-K trajectory, the Gln22 carbonyl oxygen and the amino group of the Gln22 side chain alternatively interact with the Tyr13 hydroxyl group. Try13 is the conserved residue and the experimental data indicate its important role in membrane permeabilizing activity [27]. The crystallographyc data suggest that Tyr13 is part of the glycerol-binding site [6,7]. On another hand, presence of the Tyr13 hydrophilic side chain in a peptide core may also play an important role in positioning the peptide in the lipid bilayers and water penetration and therefore membrane permeabilization [28].

Interestingly, our MD simulations show that Mg^{+2}, but not K^+ ions modify a steric environment of Tyr13 in αHTH. These results are consistent with previously reported effects of metal ions on a steric environment of Tyr13 in βPTH observed experimentally [27,29] and in the MD simulations [11]. This fact confirms the adequate representation of αHTH in our model system and reliability of computationally predicted properties.

Lastly, it should be kept in mind that the simulations were based on a computational model derived from βHTH because of unavailability of a αHTH crystal structure. On another hand, the probability of obtaining an incorrect initial structure in this case is negligible due to high sequence homology aided by strong disulfide bonding. The peptides vary at six positions where the largest changes in amino acid properties are N27G and L38G. Moreover, four disulfide bonds at the same positions within the 45 amino acid-long peptides greatly limit variability of the global structure.

5. Conclusions

Using unconstrained MD simulations we demonstrated the increased resistance of αHTH to the presence of metal ions as compared to βPTH. Changes in the primarily sequence make αHTH resistant to the presence of Mg^{+2} ions and partially increase resistance to K^+ ions. The key changes consist of replacing the ionizable residues at positions 27 and 42, which are involved in the regulating hydrogen bonding network at the C-end of the α2 helix, with glycines. As result, αHTH has the hydrogen bonding network Arg5–Arg30–Gly27, which is weaker and shorter than the corresponding network Asp42–Lys5–Arg30–Asn27 found in βPTH. Consequently, the regulating hydrogen bonding network is less sensitive to the presence of metal ions in αHTH than in βPTH. Replacement of leucine to lysine in the loop L2 reduces fluctuating motions contributing to overall stabilization of αHTH as well.

The α2 C-end is intrinsically dynamic and periodically unfolds in αHTH as in βPTH. Dynamic unfolding of the α2 C-end is guarded by the highly conserved disulphide bonds and regulated by the hydrogen bonding network involving Arg30. The mechanism of metal ion-based inhibition is similar in αHTH and βPTH and includes the unfolding of the α2 C-end and changes of dynamic and electrostatic properties.

Acknowledgments

This work was supported by LSU AgCenter Experiment Station. Simulations were performed at LSU's Center for Applied Information Technology and Learning (CAPITAL) and Biological Computation and Visualization Center (BCVC).

Appendix A. Supplementary data

Supplementary data associated with this article can be found, in the online version, at doi:10.1016/j.bpc.2007.07.005.

References

[1] B. Stec, O. Markman, U. Rao, G. Heffron, S. Henderson, L.P. Vernon, V. Brumfeld, M.M. Teeter, Proposal for molecular mechanism of thionins deduced from physicochemical studies of plant toxins, J. Pept. Res. 64 (2004) 210–224.
[2] F. Garcia-Olmedo, A. Molina, J.M. Alamillo, P. Rodriguez-Palenzuela, Plant defense peptides, Biopolymers 47 (1998) 479–491.
[3] K. Thevissen, F. Terras, W.F. Broekaert, Permeability of fungal membranes by plant defensins inhibits fungal growth, Appl. Environ. Microbiol. 63 (1999) 5451–5458.
[4] J.-A. Richard, I. Kelly, D. Marion, M. Pezolet, M. Auger, Interaction between b-purothionin and dimyristoylphosphatidylglycerol: a 31P-NMR and infrared spectroscopic study, Biophys. J. 83 (2002) 2074–2083.
[5] L. Carrasco, D. Vazquez, C. Hernandez-Lucas, P. Carbonero, F. Garcia-Olmedo, Thionins: plant peptides that modify membrane permeability in cultured mammalian cells, Eur. J. Biochem. 116 (1981) 185–189.
[6] U. Rao, B. Stec, M. Teeter, Refinement of purothionins reveals solute particles important for latice formation and toxicity. 1. a1-purothionin revisited, Acta Crystallogr., D Biol. Crystallogr. D51 (1995) 904–913.
[7] B. Stec, U. Rao, M.M. Teeter, Refinement of purothionins reveals solute particles important for lattice formation and toxicity. Part 2: structure of beta-purothionin at 1.7 angstroms resolution, Acta Crystallogr., D Biol. Crystallogr. 51 (1995) 914–924.
[8] K.A. Johnson, E. Kim, M.M. Teeter, S.W. Suh, B. Stec, Crystal structure of alpha-hordothionin at 1.9 Angstrom resolution, FEBS Lett. 579 (2005) 2301–2306.
[9] S. Van Campenhout, L. Sagi, J. Vander Stappen, G. Vlockaert, Characterisation of type-I thionin loci from the A, B, D, and R genomes of wheat and rye, Theor. Appl. Genet. 96 (1998) 80–86.
[10] P. Hughes, E. Dennis, M. Whitecross, D. Llewellyn, P. Gage, The cytotoxic plant protein, b-purothionin, forms ion channels in lipid membranes, J. Biol. Chem. 275 (2000) 823–927.
[11] S. Oard, B.B. Karki, Mechanism of β-purothionin antimicrobial peptide inhibition by metal ions: molecular dynamics simulation study, Biophys. Chemist. 121 (2006) 30–43.
[12] M. Vila-Perello, A. Sanchez-Vallet, F. Garcia-Olmedo, A. Molina, D. Andreu, Synthetic and structural studies on *Pyrularia pubera* thionin: a single-residue mutation enhances activity against Gram-negative bacteria, FEBS Lett. 536 (2003) 215–219.
[13] F. Ponz, J. Paz-Ares, C. Hernandez-Lucas, F. Garcia-Olmedo, P. Carbonero, Cloning and nucleotide sequence of a cDNA encoding the precursor of the barley toxin alpha-hordothionin, Eur. J. Biochem. 156 (1986) 131–135.
[14] S. Oard, M.C. Rush, J.H. Oard, Characterization of antimicrobial peptides against a US strain of the rice pathogen *Rhizoctonia solani*, J. Appl. Microbiol. 97 (2004) 169–180.
[15] Y. Komeiji, M. Uebayasi, Peach–Grape system — a high performance simulator for biomolecules, Chem-Bio Info. J. 2 (2002) 102–118.
[16] L.X. Dang, B.M. Pettitt, Solvated chloride-ions at contact, J. Chem. Phys. 86 (1987) 6560–6561.
[17] D.A. Pearlman, D.A. Case, J.W. Caldwell, W.R. Ross, I.T.E. Cheatham, S. DeBolt, D. Ferguson, G. Seibel, P.A. Kollman, AMBER, a computer

program for applying molecular mechanics, normal mode analysis, molecular dynamics and free energy calculations to elucidate the structures and energies of molecules, Comp. Phys. Commun. 91 (1995) 1–41.
[18] W. Kabsch, C. Sander, Dictionary of protein secondary structure: pattern recognition of hydrogen-bonded and geometrical features, Biopolymers 22 (1983) 2577–2637.
[19] W. Humphrey, A. Dalke, K. Schulten, VMD: visual molecular dynamics., J. Mol. Graph., 14 (1996) 33–38, 27–38.
[20] R.L. Dunbrack Jr., F.E. Cohen, Bayesian statistical analysis of protein side-chain rotamer preferences, Protein Sci. 6 (1997) 1661–1681.
[21] F. Bekes, R. Lasztity, Isolation and determination of amino acid sequence of avenothionin, a new purothionin analogue from oat, J. Cereal Chem. 58 (1981) 360–361.
[22] M. Fujimura, M. Ideguchi, Y. Minami, K. Watanabe, K. Tadera, Purification, characterization, and sequencing of novel antimicrobial peptides, Tu-AMP 1 and Tu-AMP 2, from bulbs of tulip (*Tulipa gesneriana* L.), Biosci. Biotechnol. Biochem. 68 (2004) 571–577.
[23] L. Vernon, G.E. Evett, R.D. Zeikus, W.R. Gray, A toxic thionin from *Pyrularia pubera*: Purification, properties and amino acid sequence, Arch. Biochem. Biophys. 238 (1985) 18–29.
[24] R. Fernandez de Caleya, C. Hernandez-Lucas, P. Carbonero, F. Garcia-Olmedo, Gene expression in alloploids: genetic control of lipopurothionins in wheat, Genetics 83 (1976) 687–699.
[25] M. Vila-Perello, A. Sanchez-Vallet, F. Garcia-Olmedo, A. Molina, D. Andreu, Structural dissection of a highly knotted peptide reveals minimal motif with antimicrobial activity, 1074/jbc.M410577200, J. Biol. Chem. 280 (2005) 1661–1668.
[26] J.W. Ponder, F.M. Richards, Tertiary templates for proteins. Use of packing criteria in the enumeration of allowed sequences for different structural classes, J. Mol. Biol. 193 (1987) 775–791.
[27] K. Wada, Y. Ozaki, H. Matsubara, H. Yoshizumi, Studies on purothionin by chemical modifications, J. Biochem. 91 (1982) 257–263.
[28] R. Sankararamakrishnan, H. Weinstein, Molecular dynamics simulations predict a tilted orientation for the helical region of dynorphin A(1–17) in dimyristoylphosphatidylcholine bilayers, Biophys. J. 79 (2000) 2331–2344.
[29] W. Fracki, D. Li, N. Owen, C. Perry, G. Naisbitt, L. Vernon, Role of Tyr and Trp in membrane responses of *Pyrularia thionin* determined by optical and NMR spectra following Tyr iodination and Trp modification, Toxicon 30 (1992) 1427–1440.